Received: 8 October 2022 | Accepted: 17 November 2022

DOI: 10.1002/pamm.202200289

Influence of Tyre Characteristics on Periodic Motions for an Understeering Vehicle

Alois Steindl[1,*], **Johannes Edelmann**[1], and **Manfred Plöchl**[1]

[1] Institute for Mechanics and Mechatronics, TU Wien, Getreidemarkt 9, 1060 Wien, Austria

We investigate the dynamics of a two-wheel vehicle model after deviating from an unstable steady powerslide motion. For a model with brush tyre characteristics we observed that for a range of constant driver inputs (front steering angle, driving torque) the motion converges to a periodic oscillation around a circular path with a very small radius of curvature. In this paper we investigate, how a modified tyre model with decreasing friction coefficient for large slip velocities influences the stability and domain of existence for these periodic motions. We also compare the obtained solutions with those using Pacejka's Magic Formula for the tyre characteristics and find a remarkable good agreement.

1 Introduction

We investigate the stationary and periodic solutions of a two-wheel vehicle model [1] shown in Fig. 1. As state variables we use the speed v, vehicle side slip angle β, yaw rate $\dot{\psi}$ and angular velocity ω_R of the rear wheel. The (constant) control parameters are given by the front steering angle δ_F and the drive torque M_R at the rear wheel. The equations of motion of the system read ([1])

$$m\dot{v}\cos\beta - m(\dot{\psi}+\dot{\beta})v\sin\beta = F_{xR} - F_{yF}\sin\delta_F, \tag{1}$$

$$m\dot{v}\sin\beta + m(\dot{\psi}+\dot{\beta})v\cos\beta = F_{yR} + F_{yF}\cos\delta_F, \tag{2}$$

$$I_\psi\ddot{\psi} = l_F F_{yF}\cos\delta_F - l_R F_{yR}, \tag{3}$$

$$I_\omega\dot{\omega}_R = M_R - r_R F_{xR}. \tag{4}$$

The horizontal tyre forces F_{yF}, F_{xR}, F_{yR} depend on the tyre slip angles α_F, α_R and are described by a modified brush model:

$$F_i = \mu_i F_{zi} f(\sigma_i/\sigma_{i,\mathrm{sat}}), \quad i \in \{F,R\},$$

where σ_i denotes the slip, $\sigma_{i,\mathrm{sat}}$ the saturation limit and

$$f(\sigma) = \begin{cases} 3\sigma - 3\sigma^2 + \sigma^3 & \text{for } \sigma \le 1 \\ \mu_{i\infty} + \frac{1-\mu_{i\infty}}{1+r_f(\sigma-1)^2} & \text{for } \sigma > 1 \end{cases}, \tag{5}$$

where $\mu_{i\infty}$ denotes the limiting value for $\sigma \to \infty$. The decay constant r_f can be estimated by comparing the function shape with Pacejka's magic formula [2], here we use $r_f = 0.25$. For $\mu_{i\infty} = 1$ we obtain the classical brush model, where the friction coefficient $f(\sigma)$ remains constant for $\sigma_i \ge \sigma_{i,\mathrm{sat}}$. The friction coefficients $\mu_i f(\sigma_i/\sigma_{i,\mathrm{sat}})$ for the choosen tyre parameters with $\mu_{i\infty} = 0.75$ are displayed in Fig. 2.

According to Fig. 1 the relative velocity $\boldsymbol{v}_{Fr}$ of the front wheel w.r.t. the direction of the wheel is given by

$$v_{Frx} = \cos\delta_F v_{Fx} + \sin\delta_F v_{Fy}, \tag{6}$$

$$v_{Fry} = \sin\delta_F v_{Fx} - \cos\delta_F v_{Fy}, \tag{7}$$

where the velocity of the front wheel is given by

$$\boldsymbol{v}_F = \begin{pmatrix} v_{Fx} \\ v_{Fy} \end{pmatrix} = \begin{pmatrix} v\cos\beta \\ v\sin\beta + l_F\dot{\psi} \end{pmatrix}.$$

Since sometimes we encounter extreme situations, where v_{Frx} becomes negative, we use the expression

$$\sigma_F = \frac{v_{Fry}}{|v_{Frx}|} \tag{8}$$

for the front slip σ_F, which gives the proper signs compared to the usually applied formula $\sigma_F = \tan\alpha_F = v_{Fry}/v_{Frx}$.

* Corresponding author: e-mail Alois.Steindl@tuwien.ac.at, phone +43 1 58801 325208, fax +43 1 58801 9325208

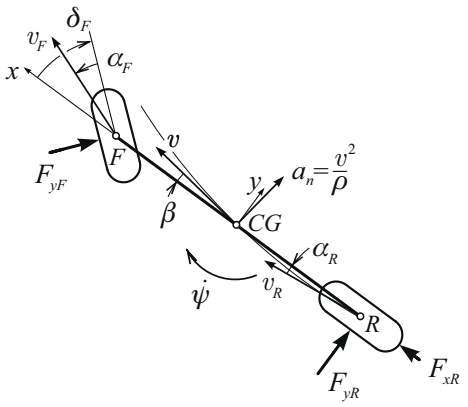

Fig. 1: Two-wheel vehicle model with state variables v, β, $\dot{\psi}$, ω_R and control parameters δ_F and M_R (not depicted).

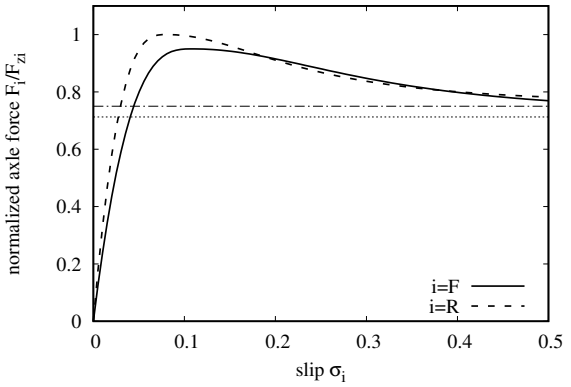

Fig. 2: Modified brush tyre model with $\mu_{i\infty} = 0.75$

For the rear slip σ_R we use

$$\sigma_R = \sqrt{v_{Rrx}^2 + v_{Rxy}^2}/(r_R\omega_R) \tag{9}$$

with the relative velocity at the contact point at the rear wheel

$$\begin{pmatrix} v_{Rrx} \\ v_{Rry} \end{pmatrix} = \begin{pmatrix} v\cos\beta - r_R\omega_R \\ v\sin\beta + l_R\dot{\psi} \end{pmatrix}.$$

Table 1: Parameters of vehicle and tyre/axle model

parameter	abbr.	value	unit
vehicle mass	m	2000	kg
vehicle yaw inertia	I_ψ	2650	$\mathrm{kg\,m^2}$
axle inertia	I_ω	6	$\mathrm{kg\,m^2}$
front axle position $\overline{CG\,F}$	l_F	1.45	m
rear axle position $\overline{CG\,R}$	l_R	1.50	m
effective tyre radius	r_R	0.35	m
front axle slip stiffness	$2c_{pF}a_F^2$	$2.6\cdot10^5$	N
rear axle slip stiffness	$2c_{pR}a_R^2$	$3.6\cdot10^5$	N
max. friction coefficient	μ_F, μ_R	0.95, 1	–

For our calculations we use the vehicle parameters displayed in Table 1, which are quite the same as in [1], except that we interchange the effective axle slip stiffness values of the front and rear tyre and consider a smaller maximum friction coefficient for the front wheel $\mu_F = 0.95$; with these parameter choices the vehicle handling behaviour becomes understeering.

1.1 Handling behaviour for the classical brush model

In Fig. 3 the control parameter δ_F depending on the speed v for the steady state of a vehicle negotiating a curve with radius $\rho = 50\,\mathrm{m}$ is depicted. The regular and overdraw steering branch of the handling behaviour for $\mu_{i\infty} = 1$ is plotted in green; it corresponds to the normal driving state in the part of the branch with 'small' steering angles. Since along this part the steering angle increases with the velocity, the vehicle is understeering; the branch is throughout stable, as typical for vehicles with understeering handling characteristics. The blue dashed curve corresponds to the powerslide manoeuvre, where the control parameter M_R is large, the vehicle side slip angle β is negative, and the front wheels point toward the outer side of the curve (the vehicle turns into a different direction compared to the steering wheel) ([3]), and the second overdraw steering branch. That branch is mostly unstable, but it contains a short part, indicated by a dotted line, where one eigenvalue vanishes. This zero eigenvalue is caused by the saturation of both tyres, such that the equations for the yaw rate $\dot{\psi}$ and the rear wheel angular velocity ω_R become linearly dependent. In the view of dynamics this situation is highly degenerate: For a given value of δ_F there exists a ray of steady motions for a certain value of M_R; for different values of M_R this branch is missing.

Fig. 4 shows the relation between δ_F and M_R along both branches for the steady cornering state. The green branch for small steering angles until the slight 'kink' at a drive torque demand of about 500 Nm corresponds to the full regular driving

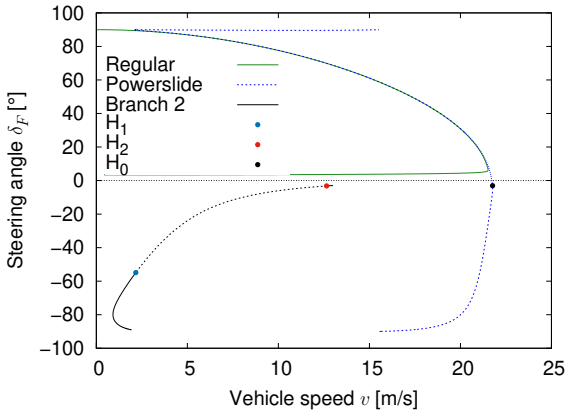

Fig. 3: Handling behaviour for the classical brush model

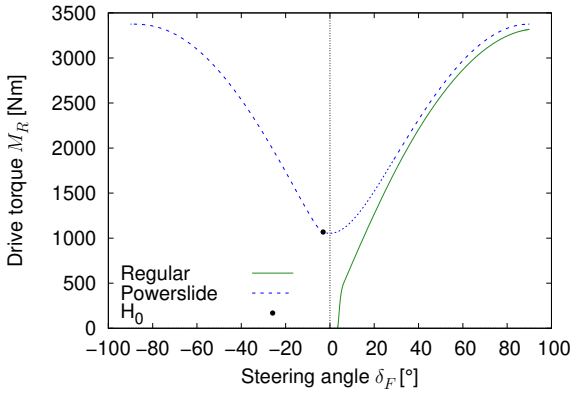

Fig. 4: Handling behaviour for the same parameters as in the left figure displaying the relation between steering angle and the driving torque

part of this branch. It becomes obvious that the drive torque demand for other steady driving conditions is considerable higher and those are thus less energy efficient.

In the diagrams below, which display the periodic solutions depending on δ_F, like e.g. Fig. 7, the corresponding value M_R on the powerslide branch is selected.

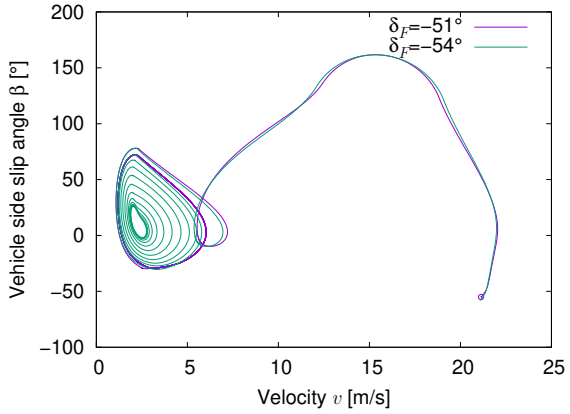

Fig. 5: Trajectories starting close to a point on the powerslide branch for different values of the steering angle δ_F

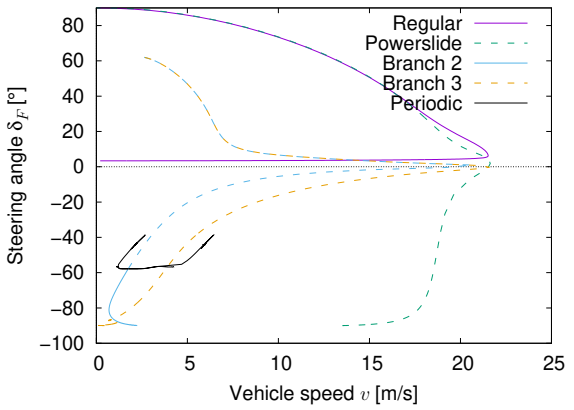

Fig. 6: Handling behaviour for the regular and powerslide branch and further stationary and periodic solution branches for the modified brush model with $\mu_{i\infty} = 0.75$.

Fig. 5 shows trajectories in (v, β)-space, which start close to a stationary point on the powerslide branch and converge to a stable periodic solution encircling a further stationary point; the coordinates of that new stationary point, which coexists with the stationary solution along the powerslide branch for the same control parameter values, is displayed as curve 'branch 2' in Fig. 3 and correspond to very small radii of curvature ('donuts'). The stationary solutions along this branch undergo Hopf bifurcations at the points H_1 and H_2, with stable stationary points at very large steering angles and corresponding drive torques from Fig. 4.

2 Existence of periodic solutions for the modified brush model with $\mu_{i\infty} = 0.75$

If the vehicle operates in a regime with large slip values ($|\sigma_i| > \sigma_{i,\mathrm{sat}}$), the tyre forces predicted by the modified brush model (5) will decay, leading to different dynamics. The corresponding handling behaviour is displayed in Fig. 6: The regular and powerslide branch look the same as in Fig. 3. The stationary velocity along the powerslide branch is shifted towards smaller speeds. As before there exists a 'branch 2' of stationary solutions, which becomes unstable for $\delta_F \approx -58°$ due to a Hopf bifurcation, and an initially supercritical family of periodic solutions bifurcates from this branch. The branch soon becomes unstable by a pair of turning points – which are visible in Fig. 6 as tiny wobbles along the lower part of the branch of periodic solutions – and a flip bifurcation, after which the unstable eigenvalue grows very rapidly in size. The unstable branch

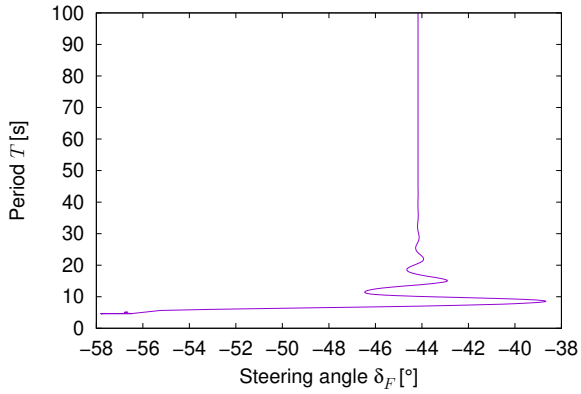

Fig. 7: Period T along the branch of periodic solutions for varying values of δ_F

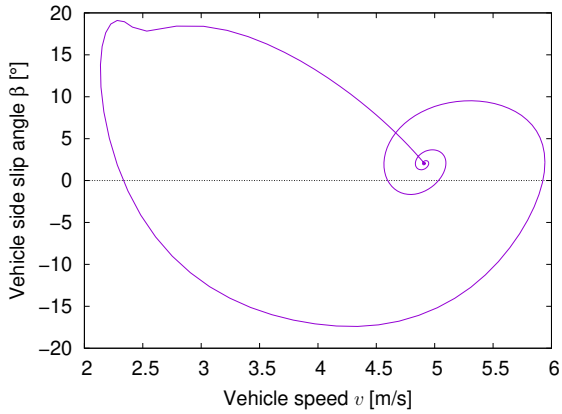

Fig. 8: Homoclinic orbit close to a Shilnikov szenario

of periodic solutions extends to $\delta_F \approx -38°$ and undergoes a sequence of turning point bifurcations until it approaches a homoclinic orbit. The period T along this branch is shown in Fig. 7; the wiggly line in this diagram indicates, that a Shilnikov szenario ([4]) occurs: As can be seen in Fig. 8, the homoclinic orbit approaches a saddle point along the stable manifold for a complex pair of stable eigenvalues and departs from the saddle along an unstable direction.

As it is explained in [5], a Shilnikov szenario can lead to strongly chaotic dynamics, because an infinite family of Smale's horseshoes occurs leading to infinitely many period doubling sequences. Since the periodic orbit in our system is already strongly unstable close to these parameter values, the chaotic dynamic doesn't occur for the considered driving parameters. Moreover, in contrast to Fig. 3, a third branch of steady conditions is found that requires further attention in forthcoming investigations.

2.1 Comparison of the results for the brush model with those for Pacejka's formula

We are now interested to compare the obtained results for the system model with the modified brush tyre model with those using an analogous setup for the basic formulation of the *Magic formula* tyre model

$$f(\sigma) = D\sin(C\arctan(B\sigma - E(B\sigma - \arctan(B\sigma)))) \tag{10}$$

by Pacejka ([2]), which is used very frequently in vehicle dynamics applications since it is able to map measured tyre characteristics while its parameters still may be interpreted w.r.t. particular tyre properties.

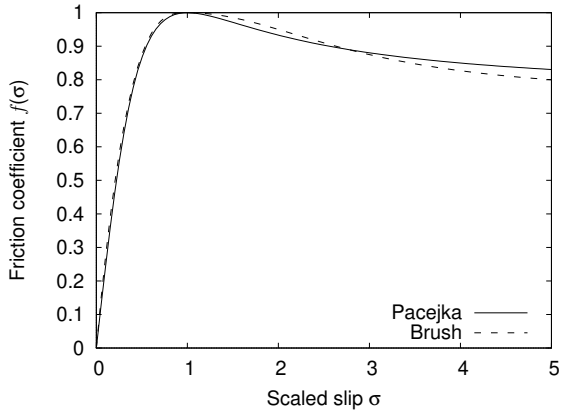

Fig. 9: Comparison of Pacejka's magic formula with the modified brush model for $\mu_{i\infty} = 0.75$

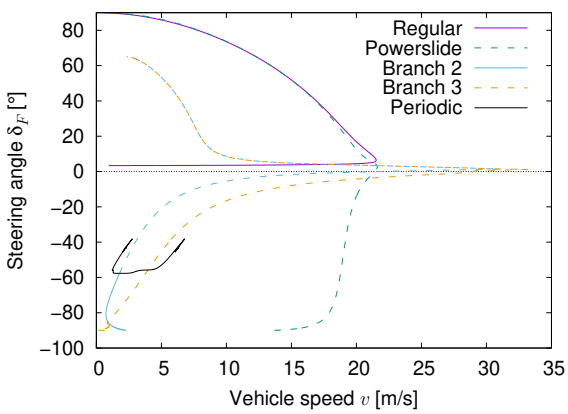

Fig. 10: Handling behaviour for the regular and powerslide branch and further stationary and periodic solution branches for Pacejka's *Magic Formula* with $\mu_{i\infty} = 0.75$.

To map the basic tyre properties, as a first step we choose the parameters B, C, D, E in (10), such that we obtain a similar limiting behaviour.

Usually E is selected close to 1, say $E = 1 - \varepsilon$; for $0 < \varepsilon \ll 1$ the function

$$y_1 = B\sigma - E(B\sigma - \arctan(B\sigma)) = \varepsilon B\sigma + (1-\varepsilon)\arctan(B\sigma)$$

rises slowly after the arctan-term is exhausted; therefore $y_2 = \arctan(y_1)$ increases from $(1-\varepsilon)\arctan(\pi/2) \approx 1.0039$ to $\pi/2$ for very large values of $B\sigma$. In order to avoid this very slow decay of $\sin(Cy_2)$ we choose $E = 1$.

Next we can select C to obtain the intended limit for $\sigma \to \infty$: With

$$C = (\pi - \arcsin(\mu_{i\infty}))\,/\,\arctan(\pi/2)$$

the function $y_3 = \sin(Cy_2)$ decays to $\mu_{i\infty}$ after it has reached the maximum value of 1. Now we can adjust B, such that y_3 reaches its maximum for $\sigma_i = \sigma_{i,\text{sat}}$:

$$C\arctan(\arctan(B\sigma_{i,\text{sat}}) = \pi/2 \quad \Rightarrow B = \tan\tan(\pi/(2C))/\sigma_{i,\text{sat}}.$$

Finally we obtain D as $\mu_i F_{zi}$.

A comparison of the two model characteristics is shown in Fig. 9 for the normalized slip $\sigma = \sigma_i/\sigma_{i,\text{sat}}$. For $\sigma \leq 1$ the functions agree almost perfectly, whereas for greater values the difference is significantly larger, but the overall shape is quite similar.

The numerical results with Pacejka's tyre model are displayed in Fig. 10. These results are in remarkably good agreement with the corresponding results shown in Fig. 6: For initial values near the powerslide branch and $\delta_F < -56°$ there exists a branch of stable stationary solutions, which attracts the trajectories. This branch undergoes a supercritical Hopf bifurcation and the periodic solutions soon become unstable due to a flip bifurcation. The periodic branch terminates at a homoclinic orbit.

2.2 Small periodic solutions for $\mu_{R\infty} = 1$ and varying values of $\mu_{F\infty}$

In this section we briefly investigate the behaviour of the vehicle, if the rear tyre is modelled with the usual brush model and the front tyre displays a decaying friction force for $|\sigma_F| > \sigma_{F,\text{sat}}$. As can be seen in Fig. 11, the periodic solutions depend

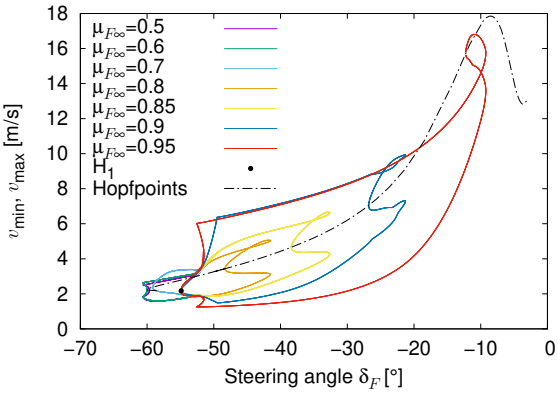

Fig. 11: Small periodic solutions for the modified brush model with $\mu_{R\infty} = 1$ and different values of $\mu_{F\infty}$

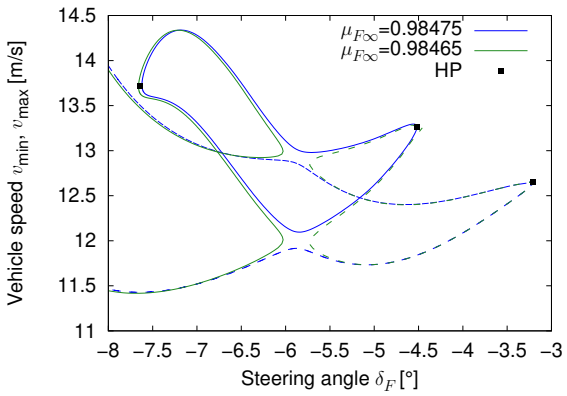

Fig. 12: Switching behaviour of periodic branches for slightly differing values of $\mu_{F\infty}$.

strongly on the parameter $\mu_{F\infty}$: For $\mu_{F\infty}$ close to 1 the periodic branch extends close to $\delta_F = 0°$, whereas for smaller values of $\mu_{F\infty}$ the branches end at Hopf bifurcation points at small values of δ_F. The location of these Hopf bifurcation points is displayed in Fig. 11 as dot-dashed curve. Since at the Hopf bifurcation point H_1 in Fig. 3 the slip σ_F at the front wheel is below the saturation value, this Hopf point and the first part of the bifurcating branch of periodic solutions is common for all branches. It should be noted, that for the displayed values of $\mu_{F\infty}$ there exists also another short branch of periodic solutions near $\delta_F = 0°$ connecting two further Hopf bifurcation points. These branches are not shown in Fig. 11, because they are hard to distinguish.

If the modified brush model approaches the classical one, i.e. for $\mu_{F\infty} \approx 1$, we observe a quite interesting switching behaviour close to the Hopfpoint H_2: As can be seen in Fig. 12, there exists also a branch of periodic solutions emanating from this Hopf point. Either this branch connects to a third Hopfpoint nearby or it is connected to the periodic solution branch from the Hopf bifurcation point H_1. The branches undergo a transcritical bifurcation for periodic solutions.

Conclusions and further research

In addition to findings from the well-known handling diagram, [2], we observed that solutions starting close to the unstable powerslide cornering motion may end up in a periodic or stationary solution corresponding to a very narrow circular path of the vehicle. These solution branches exist for a range of tyre models described by the modified brush model and depend

sensitively on the parameter values. Also when using Pacejka's tyre model these solutions have been observed and may be related to so-called 'donuts' known from race driving.

There still remains a number of open questions: For the classical brush model the periodic solution branch ends up in an orbit, which looks similar to a homoclinic orbit, but instead of a saddle point a singular manifold governs the slow dynamics.

It would of course also be of (practical) interest to study the domains of attraction of the observed solutions and learn more about the limiting behaviour of the vehicle starting at unstable initial states. Also the connections between different observed branches need more attention.

For some choices of parameters we observe states along the periodic branch, where the vehicle rotates around the touch-down point of the front wheel, while the rear wheel rotates with high speed and moves sidewards. The side slip angle β approaches $90°$ and the velocity $\boldsymbol{v}_{Fr}$ becomes very small, such that the front slip (8) behaves singularly. In this case also the brush model for the tyres needs to be modified to properly take account of the transient deformations.

In [6] we observed, that the height of the center of gravity has a strong influence on the driving behaviour, especially for situations close to stability limits. In view of these results the CG height shouldn't be neglected in the calculations, although it introduces an algebraic equation for the angular momentum balance.

Another important aspect of research is the control of the vehicle and respective trajectories, either by a human or robot driver.

Acknowledgements The authors acknowledge TU Wien Bibliothek for financial support through its Open Access Funding Program.

References

[1] Steindl, A., Edelmann, J., Plöchl, M.: Limit cycles at oversteer vehicle. Nonlinear Dynamics 99, 313-321 (2020). https://doi.org/10.1007/s11071-019-05081-8

[2] Pacejka, H.B.: Tire and vehicle dynamics. Butterworth-Heinemann, Oxford (2012)

[3] Edelmann, J., Plöchl, M.: Handling Characteristics and Stability of the Steady-State Powerslide Motion of an Automobile. Regular and Chaotic Dynamics 14, No. 6, 682-692 (2009).

[4] Shilnikov, L.P.: A case of the existence of a denumerable set of periodic motions Sov. Math. Dokl. 6, 163–166, 1965

[5] Wiggins, S.: Introduction to Applied Nonlinear Dynamical Systems and Chaos Springer-Verlag, New York, 1990.

[6] Steindl, A., Edelmann, J. and Plöchl, M. Hopf bifurcations for an oversteer vehicle – the influence of wheel load changes. *PAMM*, 21(1):e202100179, 2021. https://doi.org/10.1002/pamm.202100179

